An Optics-Based Approach to Thermal Management of Photovoltaics: Selective-Spectral and Radiative Cooling

Xingshu Sun,[1] Timothy J Silverman,[2] Zhiguang Zhou,[1] Mohammad Ryyan Khan,[1] Peter Bermel,[1] and Muhammad Ashraful Alam[1]

[1]Purdue University, West Lafayette, IN, 47907, USA

[2]National Renewable Energy Laboratory, Golden, Colorado, 80401, USA

***Abstract* - For commercial one-sun solar modules, up to 80% of the incoming sunlight may be dissipated as heat, potentially raising the temperature 20°C–30°C higher than the ambient. In the long term, extreme self-heating erodes efficiency and shortens lifetime, thereby dramatically reducing the total energy output. Therefore, it is critically important to develop effective and practical (and preferably passive) cooling methods to reduce operating temperature of PV modules. In this paper, we explore two fundamental (but often overlooked) origins of PV self-heating, namely, sub-bandgap absorption and imperfect thermal radiation. The analysis suggests that we redesign the optical properties of the solar module to eliminate parasitic absorption (*selective-spectral cooling*) and enhance thermal emission (*radiative cooling*). Our comprehensive opto-electro-thermal simulation shows that the proposed techniques would cool the one-sun and low-concentrated terrestrial solar modules up to 10°C and 20°C, respectively. This self-cooling would substantially extend the lifetime for solar modules, with the corresponding increase in energy yields and reduced LCOE.**

I. Introduction

A typical solar module converts ~20% of the incoming sunlight into electricity. Therefore, up to ~80% of the sunlight may dissipate as heat in the module, causing undesired self-heating as well as performance degradation [1], [2]. Depending on the environment, the average temperature of a solar module can be 20°C–40°C higher than the ambient. The self-heating of PV modules reduces both short-term and long-term power outputs. In the short term, the efficiencies of different PV technologies decrease with temperature, *e.g.*, the efficiency of crystalline Si modules drops by ~0.45% for every 1°C increase in temperature. In the long term, the reliability of modules suffers from thermally activated degradations, such as contact corrosion and polymer degradation, which accelerate at higher temperatures. A recent survey in India has shown that solar modules in hot climates degrade at ~1.5 %/year, eight times faster than the ones installed in cold climates (~0.2 %/year) [2]. The module lifespan was less than 15 years in hot environments, far below the 25-year standard solar panel warranty. As a result, it is important to develop effective cooling schemes to improve both the short-term and the long-term energy yields.

There are several active and passive cooling schemes already in use. These include evaporative and fin cooling [3], liquid submerged PV [4], heat pipe-based system [5], and so on [6]. *These methods cool the panels already heated by the sunlight. A scheme designed to 'prevent' or suppress self-heating could be far more effective*. Modification of the module configuration based on the fundamental physics of self-heating of PV may create a simpler, yet more effective cooling for modules.

In this context, a recent proposal involving radiative cooling of solar cells has drawn much attention [7]–[10]. However, the implication of radiative cooling for practical PV modules is not clear. For instance, Ref. [7], [8] used fused-silica as the starting point for comparison, yet fused-silica is an inferior thermal emitter compared to the commercial coverglass used in PV modules [9]. The role of electricity output of a practical solar module in determining the module temperature was also not accounted for (e.g., a slab of Si wafer instead of a solar cell was assumed in [8]–[10] and ideal solar cells at the Shockley-Queisser limit are assumed in [10]). Moreover, thermal radiation from the back side (backsheet) of solar modules was neglected in [7]–[10]. As a result, it has been difficult to ascertain the effectiveness of radiative cooling on commercial PV modules.

In this paper, we explore experimentally the physical origins of PV self-heating for a variety of solar technologies (e.g., Si, CIGS). A large fraction of elevated PV module temperature can be attributed to parasitic sub-bandgap (sub-BG) absorption as well as imperfect thermal radiation to the surroundings. Therefore, we propose to implement a sub-BG optical filter (*selective-spectral cooling*) to eliminate the parasitic absorption, and modify the top and bottom surfaces (*radiative cooling*) to enhance thermal emission. The cooling design is validated by our self-consistent opto-electro-thermal coupled simulation. We predict substantial temperature reduction for different PV materials. For example, we expect ~6 °C and ~10 °C temperature reductions in Si and CdTe solar modules, respectively. We also investigate other self-heating vulnerable PV applications, such as *low-concentration PV* (LCPV) [11] that operates at concentrated sunlight, but without the benefit of active cooling.

The paper is organized as follows. In Sec. II, we discuss the balance of energy fluxes in solar modules by introducing our opto-electro-thermal coupled framework. The underlying physics of PV self-heating is explored in Sec. III, and the corresponding optics-based cooling methods (i.e., selective-

spectral and radiative cooling) are present in Sec. IV. The cooling effectiveness is investigated in Sec. V, and its implication on both short-term and long-term energy yields is discussed in Sec. VI. Finally, we conclude the paper in Sec. VII.

II. OPTO-ELECTO-THERMAL COUPLED FRAMWORK

Energy Fluxes. A *terrestrial* PV module is subject to the following energy fluxes, see Fig. 1: 1) the absorbed solar irradiance, P_{Sun}, determined by the solar spectrum (e.g., AM1.5) as well as the absorptivity of the PV module; 2) the sky cooling, P_{Sky}, through radiative energy exchange with the atmosphere from the side facing the sky; 3) similarly, cooling due to energy transfer to the ground, P_{Ground} from the back-side; 4) convective cooling by air at the top and bottom surfaces and conductive heat transfer through the aluminum frames, $P_{Conv(d),top/bottom}$; 5) most importantly, the output power delivered by PV modules to the external load, P_{Out}.

Energy-balanced equations. For a thermodynamic system in the steady state, the incoming and outgoing energy fluxes should balance out to reach equilibrium; namely,

$$P_{Sun} = P_{Sky} + P_{Ground} + P_{Conv(d),top} + P_{Conv(d),bottom} + P_{Out}, \quad (1)$$

for terrestrial solar modules. Note that each energy flux in (1) are determined by the thermal state and optical properties of the PV modules as well as the outside environment. So one must

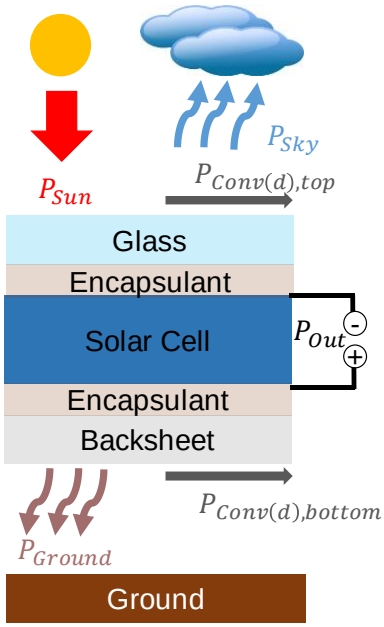

Fig. 1 Schematic of a terrestrial PV module, where we have identified the incoming and outgoing energy fluxes. Eq. (1) summarizes the energy-balance equation for the solar module.

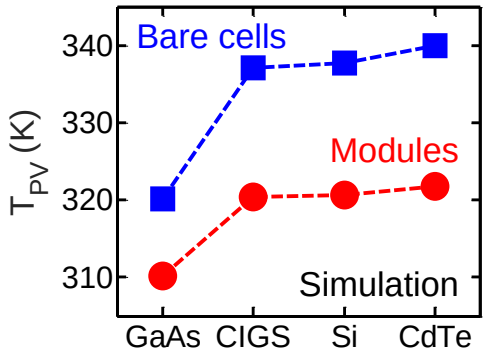

Fig. 2 The outdoor operating temperature of bare cells (blue squares) and encapsulated modules (red circles) of GaAs, CIGS, Si, and CdTe.

solve (1) opto-electro-thermally and self-consistently to calculate the steady-state temperature of PV modules. For instance, *optically,* we calculate P_{Sun} by integrating the measured absorptivity and the solar spectrum. *Thermally,* P_{Sky} depends on the temperature of PV modules, T_{PV}, and the ambient temperature, T_A, as well as the emissivity of PV modules and atmospheric transmittance in the infrared (IR) region. *Electrically*, the output power, P_{Out}, is temperature-dependent and varies among different PV technologies. Finally, the calculated temperature at equilibrium must give energy fluxes that satisfy (1). A summary of equations to calculate the energy fluxes are specified in the Appendix. Unlike the empirical approaches in [12], [13], the opto-electro-thermal simulation framework in this work can physically calculate operating temperature of modules with different solar absorbers (e.g. Si, CIGS) and various environment conditions without any fitting parameters.

Benchmark against experiments. Fig. 2 shows the temperature calculated by our opto-electro-thermal framework for different PV technologies under the same environment conditions (i.e. the wind speed is ~0.5 m/s giving an effective convective coefficient h=10 W/(K.m2) [29]; conductive heat transfer only at the module edges through metal frames is neglected; the atmospheric transmittance data is in Fig. 4; the ambient temperature T_A and solar irradiance are 300 K and 1000 W/m^2, respectively;). There are also two interesting observations from the simulated data: 1) the operating temperature varies among different PV technologies. Specifically, GaAs modules operate at much lower temperature (~310 K) compared to the others. Remarkably, our simulation anticipates the following two trends observed in the outdoor tests: (a) commercial GaAs modules operates at lower temperature (~ 10 K) compared to Si-based solar cells [14], and (b) an encapsulated module operates at lower temperature (10-20 K) compared to a bare cell without coverglass [8][8]. Indeed, these two observations can be attributed to two important self-heating mechanisms in photovoltaics: a) parasitic sub-BG absorption and b) imperfect thermal radiation, which will be discussed in detail in Sec. III.

III. PHYSICAL ORIGINS OF SELF-HEATING

A. *Parasitic sub-BG absorption*

The solar irradiance consists of photons ranging from the ultraviolet spectrum (~4 eV) to near-IR region (~0.5 eV). In general, however, only photons with energy above the bandgap excite electron-hole pairs in a semiconductor to produce electricity. For Si or CIGS solar cells ($E_G \approx 1.1$ eV), the above-bandgap spectrum accounts for ~84% of the incident solar irradiance. A module with ~18% efficiency converts part of the above-bandgap solar energy into electricity, the rest is converted to heat through carrier recombination, thermalization, and entropy generation [15]. One way to lower heat generation from above-bandgap photons is to increase the intrinsic solar cell efficiency (by multi-junction design [16], etc.), which is not discussed in this paper because we wish to focus on single-junction cells. On the other hand, for Si and CIGS, ~16% of the sunlight consists of photons with energy below the bandgap. Ideally, the sub-BG photons will not be absorbed by solar cells, rather it should be reflected back by the back metal.

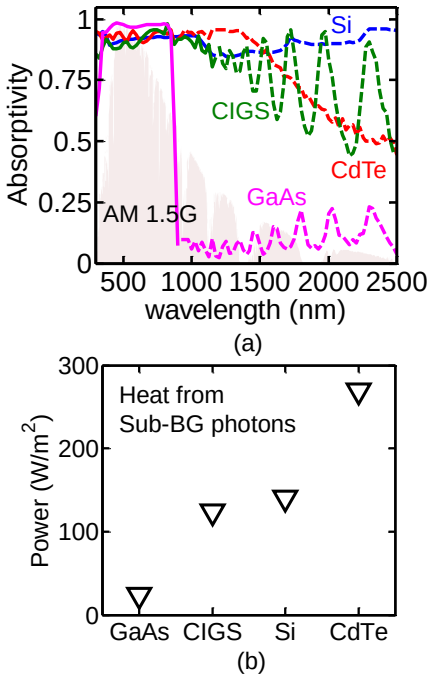

Fig. 3 (a) Measured absorptivity for different solar absorber materials vs. photon wavelength (solid lines: above bandgap photons; dashed lines: below bandgap photons). The pink area is AM1.5G spectrum. (b) Heat from sub-BG photons for different technologies.

We have measured the absorptivity profile of four different samples, with particular emphasis on the sub-BG spectrum. The optical measurements were performed using an Agilent-Cary 5000 spectrophotometer (with integrating sphere) [17] at the National Renewable Energy Laboratory (NREL). The Si sample was a commercial solar module from [14], and GaAs [18], CIGS [19] and CdTe [20] samples were fabricated at NREL lab. All the cells (except CIGS) had anti-reflection coating. The cell-level measurement, however, may underestimate the parasitic absorption slightly, because ~3% of sunlight [21] is absorbed by in the encapsulation layers of a practical module structure. Otherwise, the absorptivity profile of a module is essentially the same as that of ARC-coated bare cell, an assertion validated by our numerical modeling (not shown).

Our measurements of different PV technologies, however, show various degrees of sub-BG absorption (dashed lines in Fig. 3(a)). Specifically, Si, CIGS, and CdTe show high sub-BG absorption, while most of the below-bandgap photons are reflected in GaAs. The parasitic absorption may be variously attributed to absorbing back metal reflector, the Urbach tail, as well as free carrier absorption by highly-doped layers (emitter and back surface field in Si or window and buffer layers in CIGS and CdTe) [22]–[24]. Consequently, a large fraction of the sunlight, which consists of the sub-BG photons, now heats the solar module, see Fig. 3(b).

Among these technologies, GaAs is almost immune to sub-BG absorption possibly due to the high-quality metal mirror (gold) and reduced free carrier absorption. The magnitude of sub-BG absorption is similar between CIGS and Si (~12 % of the solar irradiance). Interestingly, CdTe has the largest parasitic absorption (~30 %) due to its larger bandgap (~1.5 eV) and strong absorptivity in the sub-BG spectrum. The consequence of sub-BG absorption among different technologies is reflected in Fig. 2, i.e., GaAs and CdTe operate at the lowest and highest temperatures, respectively. Obviously, the sub-BG absorption is not an intrinsic property of a cell technology (it can be reduced by modifying cell design, for example), therefore, the purpose of the discussion above is to highlight the importance of sub-BG absorption in determining the operating temperature of solar modules. Consequently, it is desired to eliminate the sub-BG absorption, which contributes substantially to self-heating, but not to the output power. In Sec. III, we will propose to redesign solar modules optically such that sub-BG photons are not absorbed. Next, however, we will discuss another source of self-heating, namely, imperfect thermal radiation of dissipated heat.

B. *Imperfect thermal radiation*

Thermal radiation for cooling. Another important factor dictating operating temperature of PV (T_{PV}) is the constant exchange of energy between the module and the surroundings through thermal radiation. Outdoors, solar modules receive thermal radiation from the sky and the ground; meanwhile, the top (glass) and bottom (polymer backsheet) layers of PV modules radiate to the sky and the ground, respectively. Given that the daytime module temperature is higher than the ambient, the net energy exchange from modules to surroundings is positive. Therefore, the ambient environment cools modules through thermal radiation with a spectrum peaking in the IR wavelengths. Without the cover-glass, however, solar absorbers

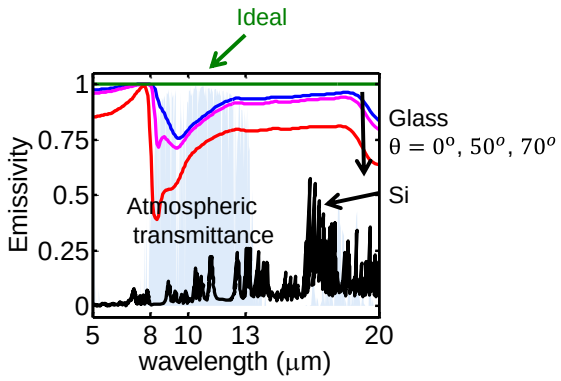

Fig. 4 Simulated emissivity profile of glass at different incident angles θ using S[4] [41]. The (n, k) data was obtained from [42]. The emissivity of Si is obtained from [7]. The ideal emissivity for radiative cooling is also shown here as green line. The blue area is the atmospheric transmittance in the zenith direction calculated by ATRAN [43] for New Delhi in spring with perceptible water vapor (PWV) = 18 mm.

can display very low emissivity in the IR spectrum, see Fig. 4. Hence, the amount of emitted thermal radiation is substantially suppressed for a bare solar cell, resulting in much higher temperature, as shown in Fig. 2. As a result, even though cell-level measurements are usually conducted indoors with heat sinks to maintain constant temperature, one must be careful to interpret the results from outdoor cell-level measurements.

Imperfect thermal radiation. Despite the fact that glass and backsheet are already highly emissive in the IR region, they are still not perfect. The emissivity of glass is calculated in Fig. 4, which shows a drop of the emissivity in the atmospheric transmission window (blue shaded area). The window corresponds to the wavelength range (8 μm –13 μm) where the atmosphere is transparent (high transmittance) to thermal emission. It is also noteworthy that the wavelengths of thermal radiation from many terrestrial objects exactly match the "transparent" window. . In other words, objects on Earth can exchange a large amount of energy with the cold troposphere (usually 50 K lower than the ambient temperature at sea level) through these wavelengths. Hence, any dip of the emissivity between 8 μm and 13 μm can lower the cooling power of a thermal emitter. Also, the emissivity of glass at higher angles reduces rapidly beyond 50°, see Fig. 4. Since thermal radiation is hemispheric (integrated with angles from 0° to 90°), the angle-dependent emissivity of glass reduces the thermal radiation from solar modules compared to an ideal emitter. Overall, the calculated average emissivity (hemispherical emissivity) of is 0.82 very close to the commercial solar glass ($\bar{\varepsilon} = 0.84$) [25], while commercial PVF backsheet has $\bar{\varepsilon} \approx 0.85$ [26], i.e., both have room for improvement. Therefore, it is desirable to re-engineer the top and bottom surfaces of solar modules to enhance thermal radiation for cooling, as we will discuss in Sec. IV.

IV. OPTICS-BASED COOLING METHODS

Thermodynamics dictate that modules must self-heat, but our focus is on avoidable temperature rise due to a) strong sub-BG absorption, b) inadequate thermal radiation. To mitigate this parasitic self-heating, we propose two optics-based cooling methods, namely, selective-spectral cooling and radiative cooling. We will briefly discuss the practical implementation or the economic viability of these cooling methods in the Sec. VI; for now, we focus on the effectiveness of the ideal designs in reducing the module temperature.

A. Selective-spectral cooling

Ideally, since the sub-BG photons do not contribute to the electricity output, they should be reflected by the cells or modules. Instead, our measurements in Fig. 3 show a large fraction of sub-BG photons are absorbed by the cell (e.g., ~300 W/m^2 for CdTe), which in turn heats up the solar module. Note that the parasitic absorption is related to the intrinsic material properties of PV modules (e.g., free carrier absorption, reflection loss), and it is not trivial to eliminate the parasitic absorption by improving absorber materials. An alternative approach may involve selective reflection the sub-bandgap photons *before* they enter the solar absorber by implementing optical filters or selective mirrors, see Fig. 5.

Ideally, the optical filter in Fig. 5(a) should be a short-pass filter, which only allows photons above E_G to pass and reflect the rest. Such a filter can be realized using quarter-wave stacks [27]. It is important that the filter does not interfere with sky-cooling, therefore, the optical filter should be inserted in between coverglass and polymer encapsulant. The filter can also be engineered to reflect the high-energy ultraviolet photons, which does not contribute efficiently to carrier generation, but cause polymer yellowing and encapsulation delamination [28] [29]. We, however, will not study or optimize for the latter.

For LCPV, side mirrors are used to concentrate sunlight onto PV modules. The widely-used metal-coated mirrors, however, have the disadvantage of reflecting the near-IR sunlight, which is dissipated as heat in PV modules. One potential improvement

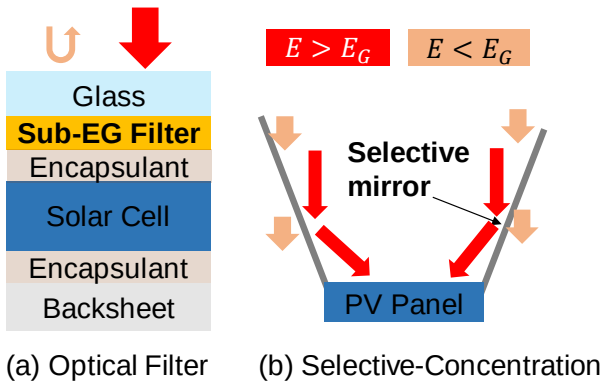

Fig. 5 Possible implementations of selective-spectral cooling by using a reflective optical filter or wavelength-selective mirror reflector for LCPV.

is to adopt wavelength-selective mirror using nanophotonics [30] or IR transmissive polymeric films [31], [32] such that only the useful photons are directed to solar modules and the rest just pass through the mirror, see Fig. 5(b). Self-heating due to sub-BG photons is therefore reduced.

B. *Radiative cooling*

As discussed in Sec. III, the top (glass) and bottom (polymer backsheet) layers of PV modules are not ideal in terms of emitting IR thermal radiation to the atmosphere and the ground. Hence, we propose to add radiative cooler layers to enhance thermal radiation from PV modules to the surroundings. The radiative cooler on top of the glass should have the ideal emissivity profile in Fig. 4 for maximum thermal emission but be transparent below 2.5 μm wavelength for solar irradiance. For objects at temperatures close to 300 K, thermal radiation shorter than 2.5 μm wavelength is negligible (~ 0.02 W/m^2 at 340 K). Hence, the transparency shorter than 2.5 μm does not sacrifice much radiative cooling power. In principle, such spectral response can be achieved using a nanophotonic crystal [8], [33]. An ideal blackbody can be used on the back surface to maximize thermal radiation exchange with the ground, but one can still use the radiative cooler for the back layer, since its performance is very close to a blackbody for IR radiation near 300 K. Note that those selective emitters which restrain thermal radiation between 8 µm and 13 μm in [34], [35] are not suitable for cooling solar modules. The hemispherical emissivity of such emitters ($\bar{\varepsilon} = 0.32$) is far below that of glass ($\bar{\varepsilon} = 0.82$), and actually would lead to higher temperature of solar modules. Those designs are only of great interest for cooling below the ambient, which solar modules illuminated under sunlight cannot achieve because solar irradiance (1000 W/m^2) is greater than thermal radiation of objects at ~300 K.

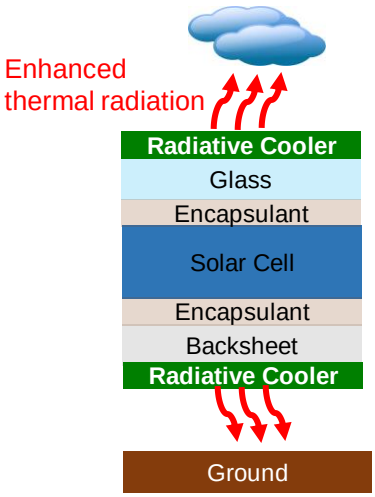

Fig. 6 Schematic of a solar module with enhanced radiative cooling.

V. Results

An interesting question is how much temperature reduction can be obtained by the two aforementioned cooling methods. To answer this question, we explored the cooling effects using our opto-electro-thermal coupled modeling framework to simulate the module temperatures with and without cooling. The simulation assumes ideal scenarios of the cooling methods (*i.e., ideal filter with cutoff at E_G for selective-spectral cooling and unity IR emissivity for radiative cooling),* which reveals the theoretical maximum reduction of temperature. We specifically study one-sun PV modules as well as LCPV.

A. *One-sun solar modules (Si, CdTe, CIGS, and GaAs)*

Fig 7 illustrates the temperature reduction (ΔT_{PV}) using the cooling schemes, compared to the module temperatures in Fig. 2. One important observation is that the selective-spectral cooling method can reduce module temperatures by ~4 K for CIGS and Si and ~8 K for CdTe, but only ~0.5 K for GaAs. This is because most of the sub-BG photons are already reflected in GaAs and further filtering these photons do not provide efficient cooling. Perfect radiative cooling provides limited cooling benefits (~1 K to 2 K reduction) compared to glass covered modules for all technologies, which agrees with the calculation in [9]. The results indicate that replacing glass ($\bar{\varepsilon} = 0.82$) and PVF backsheets ($\bar{\varepsilon} = 0.85$) with ideal thermal emitters does not result in a large decrease in the temperatures of conventional terrestrial PV modules. Later, we will demonstrate that radiative cooling can be much more effective for other PV applications. By applying both cooling schemes simultaneously, one can achieve a superposed temperature reduction. The additive cooling is understandable since these two cooling methods address different sources of PV self-heating, namely, parasitic sub-BG absorption and imperfect thermal radiation.

B. *Low Concentration PV*

Passive cooling methods are of great interest for LCPV, where no active cooling is used. With concentrated irradiance, the heat dissipated in the PV modules scales linearly with the solar concentration. As a result, the temperature of LCPV also increases linearly with concentration (e.g. ~400 K at 5-sun, see Fig. 8 (a)). Interestingly, the relative temperature reduction

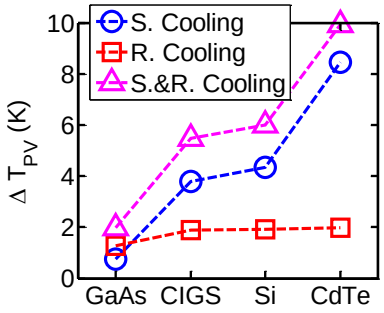

Fig. 7 Temperature reduction (with respect to module temperatures in Fig. 2) using different cooling methods for different technologies.

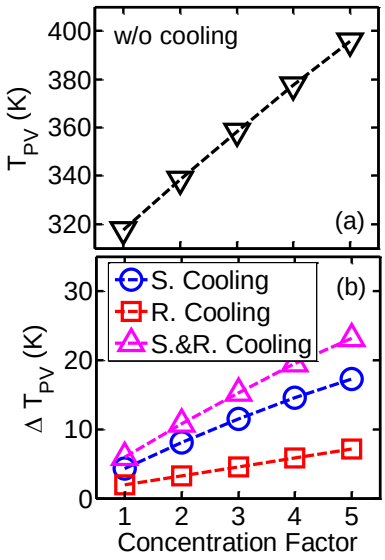

Fig. 8 (a) The operating temperature of Si-based LCPV without cooling for different concentration. (b) The temperature reduction of different cooling methods as a function of concentration factor. The boundary condition (i.e., convective coefficient, atmospheric transmittance) used here is the same as in Fig.2 and Fig. 7.

improves with concentration, as shown in Fig. 8 (b). For selective-spectral cooling, the number of sub-BG photons reflected is proportional to the concentration factor. Hence, greater cooling gains are expected at higher concentration. Thermal radiation from PV modules is proportional to $T_{PV}{}^4$, according to the Stefan–Boltzmann law. For modules at higher concentration and temperature, the radiative cooling power ($P_{Sky} + P_{Ground}$) can be substantial (~880 W/m^2 for fivefold concentration). Consequently, improving the IR emissivity using radiative cooling can much more efficient for LCPV than conventional modules. Combining selective-spectral and radiative cooling methods can provide a total temperature reduction of ~20 K for × 5 concentrated PV.

VI. Discussion

Environmental factors dictate self-cooling. So far, we have calculated T_{PV} by assuming the ambient temperature $T_A = 300$ K, an effective convective coefficient $h = 10$ W/(K.m^2) (~0.5 m/s wind speed), and the atmospheric transmittance for New Delhi in spring (Fig. 4). The remaining question is how environmental factors change the cooling effect. **First**, as h increases in a windier condition, more of the heat is lost through convection. Hence, the effectiveness of spectral and radiative cooling (reflected in absolute ΔT_{PV}, see Fig. 9 (a)) is reduced at higher wind speeds (higher h), because the excess heat is carried away by convection. Since wind speed depends on the season and the geographical location (e.g., average monthly wind-speed in New Delhi is around 4.2 m/s and 0.8 m/s in June and October, respectively [36]), the overall effectiveness of the

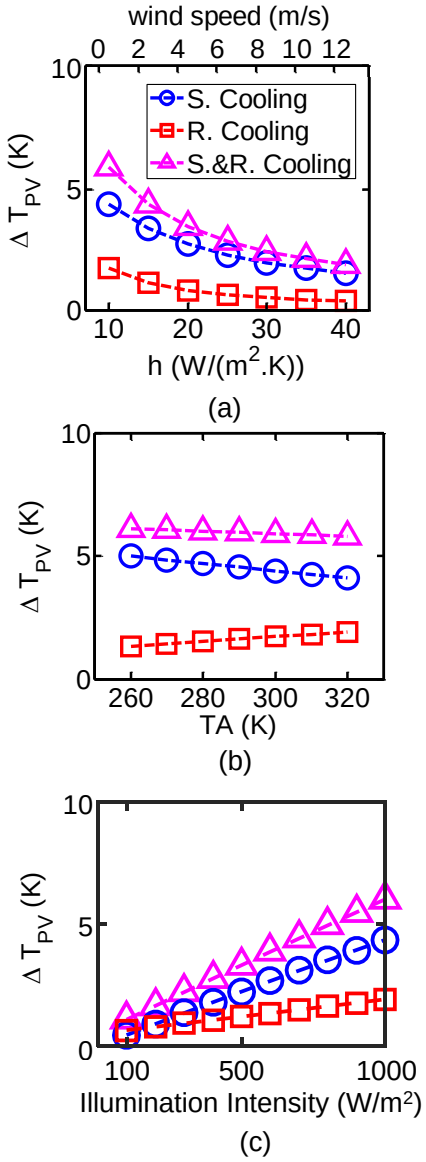

Fig. 9 Temperature reduction of conventional Si modules as a function of (a) convective coefficient/wind speed, (b) the ambient temperature, and (c) the illumination intensity. The default environment parameters for simulation are T_A = 300 K, h = 10 (W/(m^2.K)), and illumination = 1000 W/m^2. The atmospheric transmittance is taken from Fig. 4.

self-cooling strategies must be evaluated carefully for a solar farm installed in a given geographical location. **Second**, at a fixed wind speed, radiative cooling is more effective in a hotter climate as shown in Fig. 9 (b), because thermal radiation power scales with temperature as $P \sim T_{PV}{}^4$. On the other hand, intrinsic power loss (e.g., carrier recombination) increases with temperature, leading to more heat dumped from the above-bandgap irradiance. Hence, reflecting the heat power from sub-BG photons, i.e., selective-spectral cooling, is slightly less effective with increasing T_A, as shown in Fig. 9 (b). Even though selective-spectral and radiative cooling show different

trends with the ambient temperature, the cooling gain by integrating these cooling methods is almost independent of T_A. **Third**, the degree of cooling depends on the illumination intensity, see Fig. 9 (c). Since the heat dissipated in the module is reduced at lower illumination, the relative efficiency improvement by the proposed cooling techniques is also suppressed at lower illumination. **Finally**, the presence of water vapor and CO_2 reduces the transmittance between 8 μm and 13 μm of the atmosphere, directly suppressing thermal radiation from the glass encapsulation to the outer space [35]. Consequently, radiative cooling is expected to be less useful in humid and cloudy climates.

Benefits of Cooling. We have demonstrated temperature reduction of the cooling methods on different PV technologies and applications. The next obvious question is: how much energy yield gain can be achieved by cooling PV modules? For Si solar modules in terrestrial environments with an average ambient temperature of 300 K and wind speed of 0.5 m/s, the highest temperature reduction by applying the cooling methods is 6 K and 20 K for conventional module and LCPV, respectively. Given the typical temperature coefficient $\beta \approx -0.45$ %/K of Si, 6 K and 20 K can provide 2.7 % and 9 % improvements to the short-term electricity output, corresponding to 0.5 % and 1.8 % absolute increase in the efficiency of Si solar modules. Hence, the proposed cooling methods offer an alternative way to improve the efficiencies without changing the intrinsic material properties of the solar cells.

What about long-term energy gain due to self-cooling? Most degradation processes, such as moisture ingress and potential-induced degradation, are thermally activated; according to an Arrhenius relationship, the time to failure of solar modules is proportional to $\exp(-E_A/k_BT)$, where E_A is the effective activation energy and k_B is the Boltzmann constant. Using the calibrated average activation energy, $E_A = 0.89$ eV, accounting for a variety of degradation mechanisms (e.g., corrosion of interconnect, EVA yellowing, potential-induced degradation) [37] and the empirical equation for lifetime from [38], *6 K and 20 K reduction in average operating temperature can delay PV module failure due to thermally activated degradation by up to ~85% and ~290%*, respectively. As a result, selective-spectral and radiative cooling can offer significant reliability improvements and greatly reduce LCOE.

Environmental Factor. So far, the calculation of short- and long-term energy gains due to cooling has assumed a constant average ambient temperature of 300 K, solar irradiance of 1000 W/m^2, and wind speed of 0.5 m/s ($h = 10$ W/(K.m^2)). In practice, the increase of energy yield of a PV module over the course of an entire year depends on the local environment (e.g., illumination, wind speed, relative humidity, and ambient temperature). For example, the effectiveness of selective-spectral and radiative cooling is reduced at locations with high wind speed, because the module temperature is already low, and the additional benefits of selective-spectral/radiative cooling is relatively small. In addition, solar modules installed in environments with higher humidity and higher ambient temperature degrade substantially faster; hence, cooling the solar modules will significantly enhance the reliability and boost integrated energy yield. Hence, one must properly account for the geographic and temporal variation of the environmental factors to accurately predict all the incremental electricity yield by adopting the approaches discussed in this paper.

Selective-spectral vs. Radiative Cooling. Integrating selective-spectral and radiative cooling provides the most cooling advantages for solar modules, but one also needs to consider the feasibility and cost in practice. Zhu [8] has demonstrated experimentally the use of a photonic crystal (PhC) structure to improve the hemispherical emissivity for radiative cooling but the emissivity still drops substantially at higher incidence angles (Fig. 5(b) in [8]) and the hemispherical emissivity is estimated to be around 0.9, still far from unity. The fabrication cost of a nano-photonic structure also makes it an impractical option for large-scale manufacture. Additionally, though Ref. [7] argues that PhC structure can exhibit hydrophobic and self-cleaning function, the potential soiling issues from the deep air holes in PhC still need to be carefully considered especially in environments lack of rain water. Other high-emissivity coverglass applications have also been explored especially for extraterrestrial PV modules, such as pseudomorphic glass (PMG) [39]. The economic viability of adopting such a glass-technology, especially for large-scale terrestrial solar farms, remains an interesting open question.

On the other hand, selective-spectral cooling in general is more beneficial than radiative cooling, making selective-spectral cooling much more preferable. Optical filters with customized wavelength selectivity are commercially available and may be suitable for large-scale manufacturing. Including additional UV blocking in the filter can further prevent performance degradation from yellowing and delamination of encapsulants [28], [29] . The non-ideal sharpening of the filter which can degrade short circuit current and the tradeoff between cutoff sharpness and pass-band transmissivity must be carefully engineered. It also is important to note that the bandgaps of Si and GaAs decrease with temperature, characterized by the temperature coefficient (-4.73 x 10^{-4} eV/K for Si and -5.41 x 10^{-4} eV/K for GaAs), which may affect the optimal cutoff wavelength of the filter. The variation of bandgaps, however, is very small (~0.01 eV in the temperature range of interest for one-sun solar modules (300 K to 320 K). For concentrated PV with much higher operating temperature, the cutoff of the filter has to be optimized carefully to account for the temperature-dependence of bandgap. Alternative ways for selective-spectral cooling include de-texturing the front layer or nitridizing the back surface field in Si modules, both of which has been demonstrated experimentally [22], [40]. Hence, selective-spectral cooling can be more advantageous than radiative cooling for conventional solar modules, unless cost-friendly cover materials with high IR emissivity and solar transmittance are discovered. However, radiative cooling could be very effective for extraterrestrial solar modules in the absence of air convective cooling. Therefore, for both space and concentrated PV, radiative cooling remains promising to be further explored.

VII. Conclusions

To summarize, we find that self-heating in PV modules has large components due to parasitic sub-BG absorption and inadequate thermal radiation. These results are confirmed by measurements of different solar technologies (i.e., GaAs, CIGS, Si and CdTe) and outdoor tests in literature [8], [14]. To address these issues, we have proposed to optically redesign solar modules by implementing selective-spectral cooling (i.e., eliminate sub-BG parasitic photon absorption) and radiative cooling (i.e., enhance thermal radiation to the surroundings). Substantial temperature reduction has been demonstrated in different PV technologies and applications based on our self-consistently opto-electro-thermal simulation. Potentially, the temperature reduction can provide 0.5% and 1.8% absolute increase in efficiency and extend the lifetime by 80% and 260% for conventional and concentrated Si terrestrial solar modules, respectively. We also predict that selective cooling is likely to be more cost-competitive as well as more effective than radiative cooling for conventional solar modules, while the prospects of using radiative cooling in concentrated PV remains encouraging. The effectiveness of these cooling methods bring new potentials to improve reliability and performance of photovoltaics.

Acknowledgment

This work is made possible through financial support from the National Science Foundation through the NCN-NEEDS program, contract 1227020-EEC and by the Semiconductor Research Corporation, the US-India Partnership to Advance Clean Energy-Research (PACE-R) for the Solar Energy Research Institute for India and the United States (SERIIUS), U.S. Department of Energy under Contract No. DE-AC36-08GO28308 with the National Renewable Energy Laboratory, the Department of Energy under DOE Cooperative Agreement No. DE-EE0004946 (PVMI Bay Area PV Consortium), and the National Science Foundation under Award EEC1454315-CAREER: Thermophotonics for Efficient Harvesting of Waste Heat as Electricity. The authors would like to thank Dr. Dave Albin, Dr. Lorelle Mansfield, Dr. Ingrid Repins, and Dr. Myles Steiner for the measurement data, Rajiv Dubey, Shashwata Chattopadhyay, Raghu Vamsi Chavali, and Dr. Xufeng Wang for helpful discussion, and Prof. Anil Kottantharayil, Prof. Juzer Vasi, and Prof. Mark Lundstrom for kind guidance.

Appendix

In this appendix, the equation to calculate each energy flux in (1) is presented. The absorbed sunlight can be written as

$$P_{Sun} = \int_0^\infty d\lambda I_{Sun}(\lambda) \times \varepsilon(\lambda, \theta_{Sun}) \times \cos(\theta_{Sun}), \quad \text{(A1)}$$

where θ_{sun} is the solar incidence angle ($\theta_{Sun} = 0^o$ in this work), $I_{Sun}(\lambda)$ is spectral flux density of the solar spectrum at different wavelengths λ and $\varepsilon(\lambda, \theta_{Sun})$ is the absorptivity of solar modules at incidence angle θ_{sun}. For conventional solar modules, $I_{Sun}(\lambda)$ is the AM1.5G spectral density, while AM1.5 D and AM0 spectrums are used for LCPV and extraterrestrial PV, respectively.

Sky cooling power in (1) for terrestrial modules is

$$P_{Sky}(T_{PV}, T_A) = P_{Rad}(T_{PV}) - P_{Atm}(T_A). \quad \text{(A2)}$$

In Eq. (A2), $P_{Rad}(T_{PV})$, the thermal emission power radiated from the glass cover for both terrestrial and extraterrestrial modules can be expressed as

$$P_{Rad}(T_{PV}) = \int d\Omega \cos(\theta) \int_0^\infty d\lambda I_{BB}(T_{PV}, \lambda) \times \varepsilon(\lambda, \Omega). \quad \text{(A3)}$$

Here, $\varepsilon(\lambda, \Omega)$ is the angular emissivity of glass; $I_{BB}(T, \lambda) = (2hc^2/\lambda^5)/(\exp(hc/(\lambda k_B T)) - 1)$ where h is the Plank constant, c is the velocity of light, and k_B is the Boltzmann constant; $\int d\Omega = \int_0^{\pi/2} d\theta \sin(\theta) \int_0^{2\pi} d\phi$ is the angular integral over a hemisphere. Similar, $P_{Atm}(T_A)$ which is the thermal radiation from the atmosphere to PV modules can be written as

$$P_{Atm}(T_A) = \int d\Omega \cos(\theta) \int_0^\infty d\lambda I_{BB}(T_A, \lambda) \times \varepsilon(\lambda, \Omega) \times \varepsilon_{Atm}(\lambda, \Omega). \quad \text{(A4)}$$

Using Kirchhoff's law and the Beer-Lambert law [34], the angular emissivity of the atmosphere $\varepsilon_{Atm}(\lambda, \Omega)$ can be written as $\varepsilon_{Atm}(\lambda, \Omega) = 1 - t_{Atm}(\lambda)^{1/\cos(\theta)}$, where $t_{Atm}(\lambda)$ is the atmospheric transmittance in the zenith direction in Fig. 4. As pointed out in [34], the downward atmospheric spectrum can be divided into two sub-spectrums: the first one spanning 8-13 μm, and the second involving the rest of the wavelengths. The 2nd spectrum (outside the 8 -13 μm wavelength range) is emitted by water vapor and carbon dioxide within the lowest few hundred meters of the sky, at the local ambient temperature T_A. In contrast, the '8 - 13 μm spectrum' stems from the upper part of the troposphere with $T < T_A$. Hence, the atmosphere has lower spectral emissivity within 8 - 13 μm wavelength, see Fig. 3 in [34]. Because the emissivity depends on wavelength, we calculate the atmospheric radiation (see A4) by integrating the Planck's equation (at T_A) with the atmospheric emissivity, $\varepsilon_{Atm}(\lambda, \Omega)$, over the entire IR wavelength range.

Since wavelength-dependent emissivity of backsheet is not available, cooling power of thermal radiation exchange between the bottom surface and the ground (Earth) is calculated using the Stefan–Boltzmann law as

$$P_{Ground}(T_{PV}, T_A) = \sigma \varepsilon F({T_{PV}}^4 - {T_A}^4), \quad \text{(A5)}$$

where ε is the hemispherical emissivity of the back surface, F is the view factor and σ is the Stefan–Boltzmann constant. The ground temperature (could be slightly lower than T_A in practice) is assumed to be the same as the ambient temperature in this

work. The view factor is assumed to be unity for terrestrial (i.e., no tilting) solar modules in this paper.

The convective cooling power is calculated by

$$P_{Conv(d)}(T_{PV}, T_A) = h \times (T_{PV} - T_A), \quad \text{(A6)}$$

where h is the effective heat transfer coefficient combing the free and forced convection and conduction. . In this paper, the effective heat transfer coefficient, h, is set to be same for the top and bottom surfaces of solar panels assuming no tilting.

Finally, the electrical output power $P_{Out}(T_{PV})$ of the PV modules is

$$P_{Out}(T_{PV}) = P_{Out}(300\text{ K}) \times (1 + \beta \times (T_{PV} - 300\text{ K})). \quad \text{(A7)}$$

Here, for a given PV technology, $P_{Out}(300\text{ K})$ is the output power at 300 K and β is the temperature coefficient, which is negative for most solar technologies.

Coupling (A1) to (A7) into (1), one can self-consistently solve the temperature of solar modules under different environmental conditions.

REFERENCES

[1] T. J. Silverman, M. G. Deceglie, X. Sun, R. L. Garris, M. A. Alam, C. Deline, and S. Kurtz, "Thermal and Electrical Effects of Partial Shade in Monolithic Thin-Film Photovoltaic Modules," *IEEE J. Photovoltaics*, vol. 5, no. 6, pp. 1742–1747, Nov. 2015.

[2] "All-India India Survey of Photovoltaic Module Degradation : 2013."

[3] M. Chandrasekar and T. Senthilkumar, "Passive thermal regulation of flat PV modules by coupling the mechanisms of evaporative and fin cooling," *Heat Mass Transf.*, 2015.

[4] H. C. Koehler, "Cooling photovoltaic (PV) cells during concentrated solar radiation in specified arrangement in coolant with as low electric conductivity as possible," DE19904717, 2000.

[5] A. Akbarzadeh and T. Wadowski, "Heat pipe-based cooling systems for photovoltaic cells under concentrated solar radiation," *Appl. Therm. Eng.*, vol. 16, no. 1, pp. 81–87, 1996.

[6] A. ROYNE, C. J. DEY, and D. R. MILLS, "Cooling of photovoltaic cells under concentrated illumination: a critical review," *Sol. Energy Mater. Sol. Cells*, vol. 86, no. 4, pp. 451–483, Apr. 2005.

[7] L. Zhu, A. Raman, K. X. Wang, M. A. Anoma, and S. Fan, "Radiative cooling of solar cells," *Optica*, vol. 1, no. 1, pp. 32–38, 2014.

[8] L. Zhu, A. P. Raman, and S. Fan, "Radiative cooling of solar absorbers using a visibly transparent photonic crystal thermal blackbody," *Proc. Natl. Acad. Sci.*, p. 201509453, Sep. 2015.

[9] A. R. Gentle and G. B. Smith, "Is enhanced radiative cooling of solar cell modules worth pursuing?," *Sol. Energy Mater. Sol. Cells*, vol. 150, pp. 39–42, 2016.

[10] T. S. T. Safi and J. J. N. Munday, "Improving photovoltaic performance through radiative cooling in both terrestrial and extraterrestrial environments," *Opt. Express*, vol. 23, no. 19, p. A1120, 2015.

[11] "Datasheet of JN-1476-Si-Con-4x-low-concentration-PV-15-05-09." [Online]. Available: http://www.akhtersolar.com/Documents/Concentrated PV Modules/JN-1476-Si-Con-4x-low-concentration-PV-15-05-09.pdf.

[12] D. Faiman, "Assessing the outdoor operating temperature of photovoltaic modules," *Prog. Photovoltaics Res. Appl.*, vol. 16, no. 4, pp. 307–315, Jun. 2008.

[13] "Sandia Module Temperature Model." [Online]. Available: https://pvpmc.sandia.gov/modeling-steps/2-dc-module-iv/module-temperature/sandia-module-temperature-model/.

[14] T. J. Silverman, M. G. Deceglie, B. Marion, S. Cowley, B. Kayes, and S. Kurtz, "Outdoor performance of a thin-film gallium-arsenide photovoltaic module," *2013 IEEE 39th Photovolt. Spec. Conf.*, pp. 0103–0108, Jun. 2013.

[15] L. C. Hirst and N. J. Ekins-Daukes, "Fundamental losses in solar cells," *Prog. Photovoltaics Res. Appl.*, vol. 19, no. 3, pp. 286–293, May 2011.

[16] M. R. Khan and M. A. Alam, "Thermodynamic limit of bifacial double-junction tandem solar cells," *Appl. Phys. Lett.*, vol. 107, no. 22, 2015.

[17] "The Cary 4000/5000/6000i Series UV-Vis-NIR spectrophotometers." [Online]. Available: https://www.agilent.com/cs/library/brochures/5990-7786EN_Cary-4000-5000-6000i-UV-Vis-NIR_Brochure.pdf.

[18] M. A. Steiner, J. F. Geisz, I. García, D. J. Friedman, A. Duda, and S. R. Kurtz, "Optical enhancement of the open-circuit voltage in high quality GaAs solar cells," *J. Appl. Phys.*, vol. 113, no. 12, p. 123109, 2013.

[19] K. Ramanathan, M. A. Contreras, C. L. Perkins, S. Asher, F. S. Hasoon, J. Keane, D. Young, M. Romero, W. Metzger, R. Noufi, J. Ward, and A. Duda, "Properties of 19.2% efficiency ZnO/CdS/CuInGaSe2 thin-film solar cells," *Prog. Photovoltaics Res. Appl.*, vol. 11, no. 4, pp. 225–230, 2003.

[20] D. H. Rose, F. S. Hasoon, R. G. Dhere, D. S. Albin, R. M. Ribelin, X. S. Li, Y. Mahathongdy, T. A. Gessert, and P. Sheldon, "Fabrication procedures and process sensitivities for CdS/CdTe solar cells," *Prog. Photovoltaics Res. Appl.*, vol. 7, no. 5, pp. 331–340, Sep. 1999.

[21] M. R. Vogt, H. Holst, M. Winter, R. Brendel, and P. P. Altermatt, "Numerical Modeling of c-Si PV Modules by Coupling the Semiconductor with the Thermal Conduction, Convection and Radiation Equations," *Energy Procedia*, vol. 77, pp. 215–224, Aug. 2015.

[22] R. Santbergen and R. J. C. van Zolingen, "The absorption factor of crystalline silicon PV cells: A

numerical and experimental study," *Sol. Energy Mater. Sol. Cells*, vol. 92, no. 4, pp. 432–444, 2008.

[23] S. John, C. Soukoulis, M. H. Cohen, and E. N. Economou, "Theory of electron band tails and the urbach optical-absorption edge," *Phys. Rev. Lett.*, vol. 57, no. 14, pp. 1777–1780, 1986.

[24] Z. C. Holman, M. Filipič, B. Lipovšek, S. De Wolf, F. Smole, M. Topič, and C. Ballif, "Parasitic absorption in the rear reflector of a silicon solar cell: Simulation and measurement of the sub-bandgap reflectance for common dielectric/metal reflectors," *Sol. Energy Mater. Sol. Cells*, vol. 120, no. PART A, pp. 426–430, Jan. 2014.

[25] "AGC Solite Glass Datasheet." [Online]. Available: http://www.agc-solar.com/jp/agc-solar-products/patterned-glass/solite.html#uid_2_down.

[26] M. D. Bazilian, H. Kamalanathan, and D. K. Prasad, "Thermographic analysis of a building integrated photovoltaic system," *Renew. Energy*, vol. 26, no. 3, pp. 449–461, Jul. 2002.

[27] S. J. Orfanidis, *Electromagnetic Waves and Antennas*. Piscataway, NJ: Rutgers University, 2008.

[28] W. H. Holley, S. C. Agro, J. P. Galica, L. A. Thoma, R. S. Yorgensen, M. Ezrin, P. Klemchuk, and G. Lavigne, "Investigation into the causes of browning in EVA encapsulated flat plate PV modules," in *Proceedings of 1994 IEEE 1st World Conference on Photovoltaic Energy Conversion - WCPEC (A Joint Conference of PVSC, PVSEC and PSEC)*, 1994, vol. 1, pp. 893–896.

[29] A. Skoczek, T. Sample, and E. D. Dunlop, "The results of performance measurements of field-aged crystalline silicon photovoltaic modules," *Prog. Photovoltaics Res. Appl.*, vol. 17, no. 4, pp. 227–240, Jun. 2009.

[30] O. Ilic, P. Bermel, G. Chen, J. D. Joannopoulos, I. Celanovic, and M. Soljačić, "Tailoring high-temperature radiation and the resurrection of the incandescent source," *Nat. Nanotechnol.*, vol. 11, no. January, pp. 1–21, 2016.

[31] T. J. Hebrink, "Infra-red transmissive mirrors for concentrated photovoltaics," *Conf. Rec. IEEE Photovolt. Spec. Conf.*, pp. 000984–000989, 2009.

[32] J. T. Hebrink, "Durable Polymeric Films for Increasing the Performance of Concentrators," in *Third Generation Photovoltaics*, no. March, InTech, 2012, pp. 32–44.

[33] P. Bermel, S. V. Boriskina, Z. Yu, and K. Joulain, "Control of radiative processes for energy conversion and harvesting," *Opt. Express*, vol. 23, no. 24, p. A1533, 2015.

[34] C. G. Granqvist, A. Hjortsbery, and A. Hjortsberg, "Radiative cooling to low temperatures: General considerations and application to selectively emitting SiO films," *J. Appl. Phys.*, vol. 52, no. 6, p. 4205, 1981.

[35] A. P. Raman, M. A. Anoma, L. Zhu, E. Rephaeli, and S. Fan, "Passive radiative cooling below ambient air temperature under direct sunlight," *Nature*, vol. 515, no. 7528, pp. 540–544, 2014.

[36] "AVERAGE WIND SPEED IN NEW DELHI." [Online]. Available: https://weather-and-climate.com/average-monthly-Wind-speed,New-Delhi,India.

[37] K. Gregory M., Y. Shuying, and S. Ajay, "Global acceleration factors for damp heat tests of PV modules," in *IEEE 43rd Photovoltaic Specialist Conference (PVSC)*, 2016.

[38] P. Hacke, S. Spataru, K. Terwilliger, G. Perrin, S. Glick, S. Kurtz, and J. Wohlgemuth, "Accelerated Testing and Modeling of Potential-Induced Degradation as a Function of Temperature and Relative Humidity," *IEEE J. Photovoltaics*, vol. 5, no. 6, pp. 1549–1553, Nov. 2015.

[39] M. Armbruster, D. M. Wilt, R. J. Cooper, and R. C. Hoffmann, "Optical and Electrical Properties of Pseudomorphic Glass," in *IEEE 43rd Photovoltaic Specialist Conference (PVSC)*, 2016.

[40] B. P. Rand, J. Genoe, P. Heremans, and J. Poortmans, "Advanced PERC and PERL production cells with 20.3% record efficiency for standard commercial p-type silicon wafers," *Prog. Photovolt Res. Appl.*, vol. 15, no. February, pp. 659–676, 2007.

[41] V. Liu and S. Fan, "S4 : A free electromagnetic solver for layered periodic structures," *Comput. Phys. Commun.*, vol. 183, no. 10, pp. 2233–2244, Oct. 2012.

[42] M. D. Rubin, "Optical Constants and Bulk Optical Properties of Soda Lime Silica Glasses for Windows," *Sol. Energy Mater.*, vol. 12, pp. 275–288, 1985.

[43] "ATRAN," 1992. [Online]. Available: https://atran.sofia.usra.edu/cgi-bin/atran/atran.cgi.